Light-gluino scenario

V. Barger, S. Jacobs, and J. Woodside

Physics Department, University of Wisconsin, Madison, Wisconsin 53706

K. Hagiwara

Theory Group, DESY, D-2000 Hamburg-52, Federal Republic of Germany

We investigate in detail the consequences of the supersymmetry scenario with a light (~ 5 GeV) gluino and heavy (~ 100 GeV) scalar quarks, including gluino distribution and fragmentation effects, proposed to explain large-missing-p_T events observed at the CERN $p\bar{p}$ collider. The effective gluino distribution in the nucleon is evaluated using the Altarelli-Parisi equations. Ambiguities in evaluating scalar-quark production with the effective gluino distribution are discussed. A plausible gluino fragmentation function is deduced from heavy-quark fragmentation functions; scaling violations in the gluino fragmentation function are taken into account. Fragmentation effects drastically reduce the missing p_T in light-gluino jets. The present collider data do not rule out a light gluino with mass in the range of 3–5 GeV even if the $\tilde{g}$ lifetime, from decay into a photino and a quark pair, is short.

I. INTRODUCTION

Recently a supersymmetry scenario with an extra heavy scalar quark was proposed[1,2] and its predictions for missing-p_T events observed[3] at the CERN $p\bar{p}$ collider were analyzed.[2,4] In the scenario, the heavy scalar quark, with a mass on the order of 100 GeV, is produced in association with a light gluino ($m_{\tilde{g}} \approx 3-5$ GeV). The subsequent decay of the scalar quark into a quark and a photino leads naturally to monojet events with large missing p_T. A distinguishing feature of this scenario compared with other proposals[5,6] is that it predicts the dominance of monojet events over multijet events.[3]

If there does exist a light gluino ($\tilde{g}$), then high-p_T gluinos should be copiously produced via the QCD fusion processes

$$q\bar{q} \to \tilde{g}\tilde{g} , \tag{1a}$$

$$gg \to \tilde{g}\tilde{g} . \tag{1b}$$

It was suspected[5] that the subsequent decay of the gluino into a $q\bar{q}$ pair and photino would lead to a rate for large-missing-p_T events that would be incompatible with present collider data. To avoid this problem, the authors of Ref. 2 assumed that the gluino had a very long lifetime, arising from nearly degenerate gluino and photino masses. This near degeneracy of masses is unattractive from the viewpoint of grand unification theory where the photino mass is typically of order $\frac{1}{7}$ of the gluino mass,[7] in the absence of significant mixing in the neutral gaugino–Higgs-fermion sector.

In this paper we reexamine the production and decay of high-p_T gluinos taking the gluino distribution in the nucleon[8] and gluino fragmentation effects into account. We find that the missing-p_T cross section due to light-gluino decays is greatly reduced by the fragmentation effects. Consequently a long gluino lifetime is not required, and

the photino mass can be much smaller than the gluino mass.

This paper is organized as follows. In Sec. II we discuss the evaluation of the gluino distribution in the nucleon. In Sec. III the fragmentation of a gluino into a gluino hadron is analyzed. In Sec. IV we study ambiguities in the scalar-quark production cross sections obtained via the quark-gluino fusion mechanism,[1,9] $q\tilde{g} \to \tilde{q}$. Section V presents our results and conclusions. In Appendix A, we present the details of our method for obtaining scale-dependent gluino distributions in a nucleon (see also Refs. 1, 8, and 9) and gluino fragmentation functions. In Appendices B and C we give parametrizations for our gluino distribution and fragmentation functions. In Appendix D we present a derivation of a collinear approximation for $\tilde{g} \to \tilde{\gamma}$ decay used in simplifying cross-section calculations.

Near the completion of this manuscript, we received a paper by De Rújula and Petronzio[10] in which the effects of gluino fragmentation are also studied. Their fragmentation results, which are based on different calculation methods, are qualitatively similar to ours.

II. EFFECTIVE GLUINO DISTRIBUTION IN A NUCLEON

In evaluating the production of high-p_T gluinos, we must also consider the contribution that arises from the gluino distribution in a nucleon.[1,8,9] High-p_T gluinos can then be produced via the excitation processes

$$q\tilde{g} \to q\tilde{g} , \tag{2a}$$

$$g\tilde{g} \to g\tilde{g} . \tag{2b}$$

In order to determine the gluino distribution in a nucleon, we make the assumption that the distribution vanishes at values of Q below the gluino mass scale:

$$\tilde{g}(x, Q \le Q_0 = nm_{\tilde{g}}) = 0 . \tag{3}$$

This condition follows from the general argument[11] of the decoupling of heavy particles at low energies, but the choice of n is rather arbitrary as long as $n \sim (1)$. We take $n = 2$ as our standard choice and discuss the related ambiguities in Sec. IV.

If we ignore bottom- and top-quark as well as scalar-quark contributions, the Q^2 evolution of the parton distributions is governed by the equations[8,12]

$$\frac{dq_i}{d\bar{s}} = (\tilde{b})^{-1}(P_{qq} \otimes q_i + P_{qg} \otimes g) , \tag{4a}$$

$$\frac{dg}{d\bar{s}} = (\tilde{b})^{-1}(P_{gq} \otimes q_s + P_{gg} \otimes g + P_{g\tilde{g}} \otimes \tilde{g}) , \tag{4b}$$

$$\frac{d\tilde{g}}{d\bar{s}} = (\tilde{b})^{-1}(P_{\tilde{g}g} \otimes g + P_{\tilde{g}\tilde{g}} \otimes \tilde{g}) , \tag{4c}$$

where $q_i = q_i(x,\bar{s})$ is the ith-quark distribution, $i = u, \bar{u}, d, \bar{d}$, etc., $q_s \equiv \sum_{i=1}^{2f} q_i$ with $f = 4$, $g = g(x,\bar{s})$ and $\tilde{g} = \tilde{g}(x,\bar{s})$ are gluon and gluino distributions, respectively, $b = (33 - 2f - 6)/6 = \frac{19}{6}$, and

$$\bar{s} = \ln[\ln(Q/\tilde{\Lambda})/\ln(Q_0/\tilde{\Lambda})] . \tag{5}$$

In cross-section calculations we take $Q = (\hat{s})^{1/2}$, the subprocess c.m. energy. The value of $\tilde{\Lambda}$ is determined by the choice of the QCD scale parameter Λ_4 for four flavors ($f = 4$) and by requiring continuity of α_s as the gluino threshold is crossed; $\tilde{\Lambda} = Q_0(\Lambda_4/Q_0)^{25/19}$ with $\Lambda_4 = 0.2$ GeV. The various P_{ab} are the so-called splitting functions whose explicit forms can be found in Refs. 8 and 12. The $\otimes$ product is defined by

$$f \otimes g = \int_x^1 \frac{dy}{y} f\left(\frac{x}{y}\right) g(y) . \tag{6}$$

We solve Eqs. (4) by first integrating over $\bar{s}$ and then using the method of successive approximations[13] (see Appendix A for details) with the Eichten-Hinchliffe-Lane-
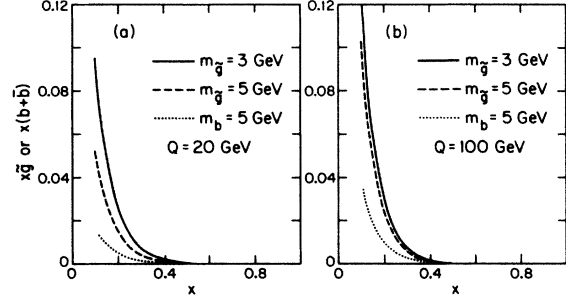

FIG. 1. Effective gluino distribution in a nucleon at (a) $Q = 20$ GeV and (b) 100 GeV for $m_{\tilde{g}} = 3$ GeV (solid curves) and 5 GeV (dashed curves) with $Q_0 = 2m_{\tilde{g}}$ as the decoupling momentum scale. Also shown as dotted curves are the effective bottom-quark distribution $(b + \bar{b})$ obtained by Hagiwara and Jacobs (Ref. 14).

Quigg (EHLQ) set I parametrization[14] for the initial light-quark and gluon distributions. We show in Fig. 1 the gluino distributions at $Q = 20$ and 100 GeV for $m_{\tilde{g}} = 3$ and 5 GeV. Also shown are bottom-quark distributions $(b + \bar{b})$ obtained by using the same initial distributions[14] and $b, \bar{b}$ decoupling conditions corresponding to Eq. (3). Note that the gluino distribution for $m_{\tilde{g}} = 5$ GeV $(= m_b)$ is more than twice as large as the sum of the b and $\bar{b}$ distributions, due to the large color factor $T_A = 3$ in the splitting function $P_{\tilde{g}g}$ as compared to $T_F = \frac{1}{2}$ in P_{qg}.

Simple parametrizations for the gluino distributions are presented in Appendix B. We find that the light-quark and gluon distributions change by less than 15% by the introduction of the gluino. Hence, we do not reparametrize these distributions but use the EHLQ parametrizations given in Ref. 14.

Finally, we note that the differential cross sections for the subprocesses of Eqs. (2) can be obtained from the results for the fusion subprocesses given in Ref. 4 by crossing:

$$\frac{d\hat{\sigma}}{dt}(q\tilde{g} \to q\tilde{g}) = \frac{\pi\alpha_s^2}{s^2}\left[\frac{4}{9}\left[\frac{s^2}{(\mu^2-s)^2+\mu^2\Gamma^2} + \frac{u^2}{(\mu^2-u)^2}\right] - \frac{s^2(\mu^2-s)}{t[(\mu^2-s)^2+\mu^2\Gamma^2]} - \frac{u^2}{t(\mu^2-u)} + \frac{t^2+u^2}{t^2}\right] , \tag{7a}$$

$$\frac{d\hat{\sigma}}{dt}(g\tilde{g} \to g\tilde{g}) = \frac{9\pi\alpha_s^2}{4s^2}\left[\frac{s^2+u^2}{t^2} - \frac{u}{s} - \frac{s}{u}\right] . \tag{7b}$$

Here $\mu = m_{\tilde{q}}$ and the gluino mass has been neglected; Γ is the total scalar-quark width, estimated[2,4] to be $\Gamma \simeq 9$ GeV for $m_{\tilde{q}} = 100$ GeV.

III. GLUINO FRAGMENTATION FUNCTION

The Q^2 evolution of the gluino fragmentation function is determined by[15]

$$\frac{dD_{\tilde{g}}}{d\bar{s}} = (\tilde{b})^{-1}P_{\tilde{g}\tilde{g}} \otimes D_{\tilde{g}} . \tag{8}$$

In order to solve Eq. (8) for $D_{\tilde{g}} = D_{\tilde{g}}(z,\bar{s})$, we need to know the initial gluino fragmentation function. Peterson,

Schlatter, Schmidt, and Zerwas[16] suggested the form

$$D_Q(z) = \frac{Nz(1-z)^2}{[(1-z)^2+\epsilon_Q z]^2} \tag{9}$$

for heavy-quark fragmentation. Here we choose $z = \hat{p}/\hat{p}_{max}$ with $\hat{p}$ the momentum of the heavy-quark hadron in the center-of-mass frame of the hard-scattering process; N is a normalization constant fixed by the condition

$$\int_0^1 dz\, D(z) = 1 . \tag{10}$$

It was argued in Ref. 16 that the parameter ϵ_Q should be

proportional to $1/m_Q{}^2$. We use Eq. (9) as our gluino fragmentation function at Q_0 and consider two choices for $\epsilon_{\tilde{g}}$:

$$\epsilon_{\tilde{g}} = \epsilon_b (m_b/m_{\tilde{g}})^2 , \qquad (11a)$$

$$\epsilon_{\tilde{g}} = \tfrac{9}{4}\epsilon_b (m_b/m_{\tilde{g}})^2 . \qquad (11b)$$

The factor $\tfrac{9}{4}$ in Eq. (11b) assumes a string tension for a color-octet gluino that is $\tfrac{9}{4}$ times larger than the string tension for a color-triplet quark. We use the value $\epsilon_b = 0.008$ from an evolved fit to b-quark fragmentation data (see Ref. 17 for a recent compilation of data).

With these initial fragmentation functions, we solve Eq. (8) using the method of successive approximations.[13] In Fig. 2 we show the fragmentation functions at $Q = 40$ GeV for $m_{\tilde{g}} = 3$ and 5 GeV. Solid curves are obtained by the initial distributions with Eq. (11a), while dashed curves are obtained by those with Eq. (11b). Comparison is made with the bottom-quark fragmentation function at the same value of Q. Note that the initial form of the bottom-quark and the gluino fragmentation functions are identical at $m_{\tilde{g}} = 5$ GeV ($= m_b$) for the choice of Eq. (11a). The difference between the b and $\tilde{g}$ results at $Q = 40$ GeV demonstrates the striking difference in the gluon radiation effects between the color-octet gluino (with color factor $C_A = 3$ in the splitting function $P_{\tilde{g}\tilde{g}}$) and the color-triplet heavy quarks (with the color factor $C_F = \tfrac{4}{3}$ in P_{qq}). The $\tilde{g}$ fragmentation is appreciably softer than b fragmentation. We present parametrizations for the various gluino fragmentation functions in Appendix C.

IV. UNCERTAINTIES IN $\sigma(\tilde{q})$

In Refs. 2 and 4, the scalar-quark production cross section was evaluated via the subprocess

$$qg \to \tilde{q}\,\tilde{g} . \qquad (12)$$

In the limit

$$m_{\tilde{g}}/m_{\tilde{q}} \to 0 \qquad (13)$$

the total cross section from the subprocess (12) diverges logarithmically. By summing over all the leading logarithms, we obtain the effective gluino distribution in a nucleon (see Sec. II) and the $\tilde{q}$ production cross section can be evaluated via the fusion process

$$q\tilde{g} \to \tilde{q} . \qquad (14)$$

The latter method was chosen in Refs. 1 and 9.

In this section, we compare the scalar-quark production cross sections obtained via the above two methods and attempt to determine which to rely upon. We assume throughout that the scalar quarks associated with left- and right-handed quarks are degenerate. Figure 3 shows the scalar-quark production cross section in $p\bar{p}$ collision at $\sqrt{s} = 540$ GeV calculated by the two methods for $m_{\tilde{q}} = 100$ GeV and variable $m_{\tilde{g}}$. The solid curve denotes the cross section obtained via (12) and the dashed curves are obtained via (14). The $m_{\tilde{g}}$ dependence of the cross section in the $q\tilde{g} \to \tilde{q}$ calculations enters only through the difference in the $\tilde{g}$ distribution, which in turn is determined by the decoupling mass scale $Q_0 = nm_{\tilde{g}}$ in Eq. (3). Results obtained with setting $n = 1$, 2, and 4 are shown.

It is striking that the fusion process (14) gives a rather large cross section, as previously found in Refs. 1 and 9. The desired[3] cross section of order 2 nb, which corresponds to a few monojet events per 100 nb^{-1} at the CERN collider, is obtained for $m_{\tilde{g}} \sim 5$ GeV in the $qg \to \tilde{q}\tilde{g}$ calculation, whereas the same cross section occurs for $m_{\tilde{g}} \sim 20$ GeV in the $q\tilde{g} \to \tilde{q}$ calculation with $Q_0 = 2m_{\tilde{g}}$. The discrepancy between the two calculational methods does not disappear even with the severe threshold condition $Q_0 = 4m_{\tilde{g}}$. On the other hand, it is rather difficult to accept that the naive perturbation theory based on
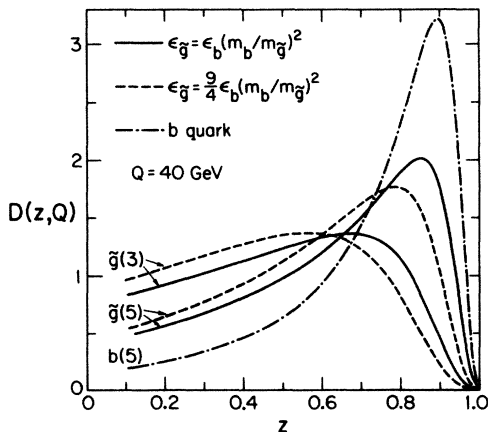

FIG. 2. Effective gluino fragmentation function at $Q = 40$ GeV with the initial parametrization given by $\epsilon_{\tilde{g}}$ of Eq. (11a) (solid curves) and Eq. (11b) (dashed curves). Also shown as a dash-dotted curve is the effective bottom-quark fragmentation function at $Q = 40$ GeV.
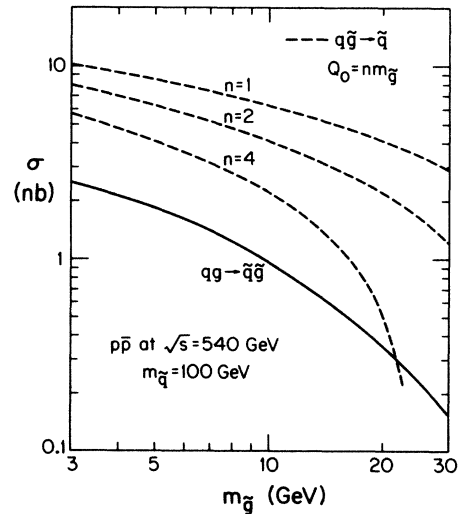

FIG. 3. Scalar-quark production cross section in $p\bar{p}$ collision at $\sqrt{s} = 540$ GeV for $m_{\tilde{q}} = 100$ GeV versus $m_{\tilde{g}}$. The solid curve denotes the result obtained via the lowest-order $qg \to \tilde{q}\tilde{g}$ subprocess and dashed curves denote those obtained via $q\tilde{g} \to \tilde{q}$ fusion with the $\tilde{g}$ distributions being determined through the matching condition of Eq. (3) with $Q_0 = nm_{\tilde{g}}$; $n = 1$, 2, and 4. The set I parametrizations of Ref. 14 were used as the initial parton distributions.

the $qg \rightarrow \tilde{q}\,\tilde{g}$ process fails for $m_{\tilde{g}} > 10$ GeV, because then the logarithmic factor $\ln(m_q^2/m_{\tilde{g}}^2)$ is not overwhelmingly large.

In order to clarify the problem, we compare the two calculational methods in more detail by making several simplifying approximations. We ignore both scaling violations in the running coupling constant and the parton distribution functions. We take for definiteness $\alpha_s(Q) = \alpha_s(m_{\tilde{q}})$, $g(x) = g(x, m_{\tilde{q}})$, and $q(x) = q(x, m_{\tilde{q}})$. We further ignore the gluon radiation from the gluino. Then the Altarelli-Parisi (AP) equation for the gluino distribution simplifies to

$$Q \frac{\partial}{\partial Q} \tilde{g}(x, Q) = \frac{\alpha_s}{\pi} P_{\tilde{g}g} \otimes g \tag{15}$$

which is readily integrated to give

$$\tilde{g}(x, m_{\tilde{q}}) = \left[\frac{\alpha_s}{\pi} \ln \frac{m_{\tilde{q}}}{Q_0} \right] P_{\tilde{g}g} \otimes g . \tag{16}$$

Equation (16) allows the interpretation that the gluino distribution in a gluon is proportional to the splitting function $P_{\tilde{g}g}$. In this approximation, the $qg \rightarrow \tilde{q}\,\tilde{g}$ cross section can be obtained by the convolution of the $\tilde{g}$ distribution in the gluon with the $q\tilde{g} \rightarrow \tilde{q}$ fusion cross section:

$$\hat{\sigma}(qg \rightarrow \tilde{q}\,\tilde{g})_{\mathrm{E\tilde{g}A}} = \frac{\pi \alpha_s^2}{\hat{s}} \ln \frac{m_{\tilde{q}}}{Q_0} \left[\left[1 - \frac{m_{\tilde{q}}^2}{\hat{s}} \right]^2 \right.$$
$$\left. + \left[\frac{m_{\tilde{q}}^2}{\hat{s}} \right]^2 \right] . \tag{17}$$

This is an "equivalent-gluino approximation"[18] (E$\tilde{g}$A) to the exact cross section obtained by integration of the lowest-order differential cross section (see Appendix A of Ref. 4)

$$\hat{\sigma}(qg \rightarrow \tilde{q}\,\tilde{g})_{\mathrm{EXACT}} = \int_{t_-}^{t_+} d \, |t| \, \frac{d\hat{\sigma}}{d \, |t|} \tag{18}$$

with

$$t_\pm = \tfrac{1}{2} \{ s - m_{\tilde{q}}^2 - m_{\tilde{g}}^2 \pm [(s - m_{\tilde{q}}^2 - m_{\tilde{g}}^2)^2$$
$$- 4 m_{\tilde{q}}^2 m_{\tilde{g}}^2]^{1/2} \} . \tag{19}$$

We find that the coefficient of the logarithmic part in $\hat{\sigma}_{\mathrm{EXACT}}$ agrees with that of $\hat{\sigma}_{\mathrm{E\tilde{g}A}}$ and $\hat{\sigma}_{\mathrm{E\tilde{g}A}}$ gives a reasonable approximation well above the threshold, $(\hat{s})^{1/2} = m_{\tilde{q}} + m_{\tilde{g}}$.

The total cross section in $p\bar{p}$ collisions is obtained by convoluting the subprocess cross section $\hat{\sigma}$ with the luminosity functions

$$\sigma(p\bar{p} \rightarrow \tilde{g}x) = \int d\tau \frac{d\mathscr{L}}{d\tau} \hat{\sigma}(\hat{s} = s\tau)$$

$$= \int d(\hat{s})^{1/2} \frac{2(\hat{s})^{1/2}}{s} \frac{d\mathscr{L}}{d\tau} \hat{\sigma}(\hat{s} = s\tau) , \tag{20}$$

where

$$\frac{d\mathscr{L}}{d\tau} = \int_\tau^1 \frac{dx}{x} q(x) g \left[\frac{\tau}{x} \right] . \tag{21}$$

Here we neglect the quark distribution in $\bar{p}$. Figures 4(a) and 4(b) show the product of the luminosity function and the subprocess cross sections $\hat{\sigma}_{\mathrm{EXACT}}$ and $\hat{\sigma}_{\mathrm{E\tilde{g}A}}$, respectively, versus $(\hat{s})^{1/2}$. The normalizations are such that the the area under each curve is the total cross section. Because the luminosity function drops very rapidly with $(\hat{s})^{1/2}$, roughly an order of magnitude or more per 50 GeV, contributions from the threshold region are very important, where the E$\tilde{g}$A is inapplicable. The difference in the total cross section obtained with different $\hat{\sigma}$ is striking for sizable $m_{\tilde{g}}$, e.g., the area under the $\hat{\sigma}_{\mathrm{E\tilde{g}A}}$ curve with $m_{\tilde{g}} = 20$ GeV is comparable to the area under the $\hat{\sigma}_{\mathrm{EXACT}}$ curve with $m_{\tilde{g}} = 5$ GeV. Despite the fact that our E$\tilde{g}$A picks up only a single logarithm [see Eq. (17)], whereas the AP equations sum over all the leading logarithms, we reproduce qualitatively the effect of the full AP equations.

The physical-threshold cutoff at $(\hat{s})^{1/2} = m_{\tilde{q}} + m_{\tilde{g}}$ on the $qg \rightarrow \tilde{q}\,\tilde{g}$ subprocess cross section is not imposed in the AP calculation. A large cross-section enhancement in the AP calculation results from the rapid rise of the luminosity function between $(\hat{s})^{1/2} = m_{\tilde{q}} + m_{\tilde{g}}$ and $(\hat{s})^{1/2} = m_{\tilde{q}}$. Consequently we are led to conclude that the scalar-quark production cross section calculated via $q\tilde{g} \rightarrow \tilde{q}$ fusion with the AP-generated gluino distribution is an overestimate. Therefore, we choose to use only the lowest-order QCD perturbative calculation for $qg \rightarrow \tilde{q}\,\tilde{g}$ with the possibility of a radiative correction of order of a factor of 2. Similarly, we do not include the contribution from subprocess (2a) when the scalar quark can be produced as a real particle, but instead calculate $qg \rightarrow \tilde{q}\,\tilde{g}$ production with $\tilde{q} \rightarrow q\tilde{g}$ decay.

We repeated the same analysis using the modified AP equation with threshold suppression introduced by Glück, Hoffman, and Reya[19] and employed by EHLQ (Ref. 14). We found qualitatively similar results; the $\tilde{g}$ distribution obtained from these modified AP equations again gives an overestimate of the $\tilde{q}$ production cross section. The threshold suppression carefully arranged[19] for heavy-quark contributions to the electroproduction structure
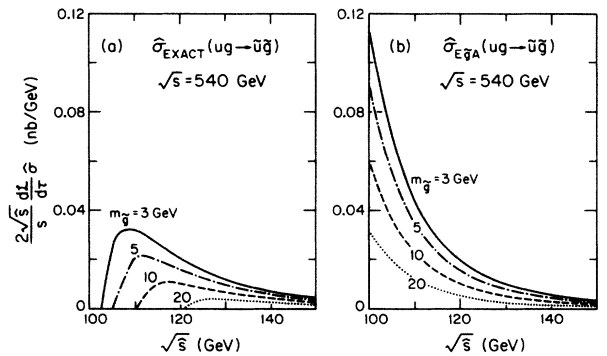

FIG. 4. Product of the subprocess cross section $\hat{\sigma}(ug \rightarrow \tilde{u}\,\tilde{g})$ and the luminosity function for $m_{\tilde{u}} = 100$ GeV plotted against $(\hat{s})^{1/2}$ with (a) $\hat{\sigma}_{\mathrm{EXACT}}$ and (b) $\hat{\sigma}_{\mathrm{E\tilde{g}A}}$, as defined in the text. The normalization is such that the area under each curve gives the total $\tilde{u}$ production cross section summed over two chiralities. Solid, dash-dotted, dashed, and dotted curve represent $m_{\tilde{g}} = 3, 5, 10,$ and 20 GeV, respectively.

function does not account for the threshold suppression in hadronic processes.

The study presented in this section is relevant more generally to the question of when the leading-logarithmic approximation is reliable. The success of the equivalent W approximation[20] for the production of very heavy Higgs bosons at TeV collider energies may in part be due to the fact that no extra massive particles are produced in the subprocess.

V. RESULTS AND CONCLUSIONS

Figure 5 shows the missing-P_T distribution from $p\bar{p}$ collisions at $\sqrt{s} = 540$ GeV obtained from the subprocess in Eqs. (1) and (2) without fragmentation and with fragmentation given by Eqs. (11) for $m_{\tilde{g}} = 5$ GeV with infinite $m_{\tilde{q}}$. For the $\tilde{g}_h$ decay into $\tilde{\gamma}$, we use the collinear approximation presented in Appendix D. The fragmentation effect substantially decreases the $\not{p}_T$ contributions at high $\not{p}_T$ even for the conservative parametrization of Eq. (11a). We note that the contribution from the excitation processes of Eqs. (2) are typically 75% of the total at $\not{p}_T = 35$ GeV, but their fraction decreases precipitously at higher $\not{p}_T$.

Figure 6 shows the missing-p_T distribution summed over various contributions: $\tilde{q}\,\tilde{g}$ production followed by $\tilde{q} \to q\tilde{\gamma}$ and $\tilde{q} \to q\tilde{g}$ decay, $\tilde{g}\,\tilde{g}$ production (1) and $g\tilde{g}$ scattering (2b). Here we have set $m_{\tilde{q}} = 100$ GeV, $m_{\tilde{g}} = 5$ GeV, and $m_{\tilde{\gamma}} = 0$. The $\tilde{q} \to q\tilde{\gamma}$ decay contribution alone is shown separately. With the $\tilde{g} \to \tilde{g}_h$ fragmentation effect included the extra contributions are significant only in the region $\not{p}_T < 40$ GeV.

Figure 7 shows monojet and dijet event cross sections as a function of the gluino mass obtained by summing all the contributions. The event selection criteria are explained in
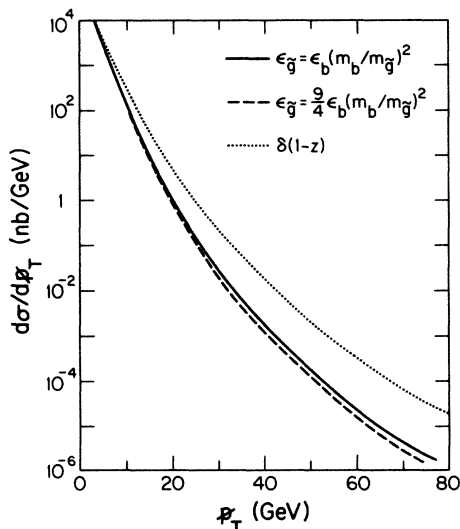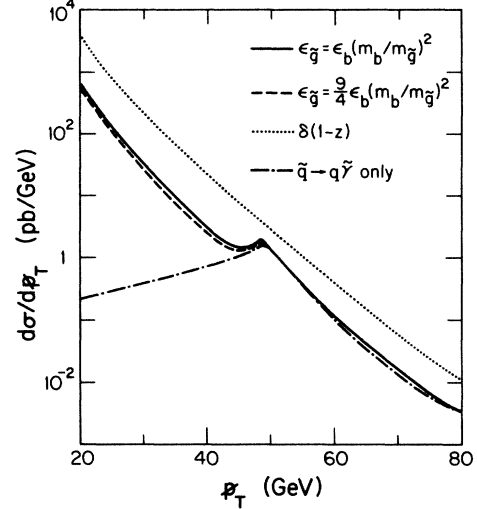
FIG. 6. Missing-p_T distribution in $p\bar{p}$ collisions at $\sqrt{s} = 540$ GeV for $m_{\tilde{q}} = 100$ GeV, $m_{\tilde{g}} = 5$ GeV, and $m_{\tilde{\gamma}} = 0$ summed over the contributions from $\tilde{q}\,\tilde{g}$ production (followed by $\tilde{q} \to q\tilde{\gamma}$ or $\tilde{q} \to q\tilde{g}$ decays), $\tilde{g}\,\tilde{g}$ production (1) and $g\tilde{g}$ scattering (2b). The curves are obtained by using the effective fragmentation functions of Eq. (11a) (solid curve), Eq. (11b) (dashed curve), or neglecting fragmentation (dotted curve). Also shown is the contribution from $\tilde{q} \to q\tilde{\gamma}$ decay only (dash-dotted curve).

detail in Ref. 4. We require that $\not{p}_T > \max(35 \text{ GeV}, 4\sigma)$ with σ being the UA1 $\not{p}_T$ resolution. We further require that the jet p_T exceed 12 GeV with the highest jet above 25 GeV. The $\not{p}_T$ trigger condition is chosen in order to avoid sensitivity to spectator-scalar-E_T estimates. The contribution in the region $15 < \not{p}_T < 35$ GeV is found to be rather sensitive to the spectator jet activities and may not be used as a reliable guide to reject particular supersymmetry contributions on a quantitative basis.

For a gluino mass greater than 5 GeV, we neglect excitation contributions (2) as well as the scaling violation in the gluino fragmentation function and evaluate the $\tilde{g} \to q\bar{q}\,\tilde{\gamma}$ decay exactly without using the collinear approximation. Figure 7 shows the cross sections obtained with no $\tilde{g} \to \tilde{g}_h$ fragmentation, as well as with the choices in Eqs. (11). With fragmentation included, the event rates fall at $m_{\tilde{g}} < 20$ GeV. Hence in the scenario of Refs. 1 and 2 ($m_{\tilde{g}} = 3-5$ GeV), there is no need to require near degeneracy of $m_{\tilde{g}}$ and $m_{\tilde{\gamma}}$ to make $\tilde{g}$ lifetime long.

The cross sections in Fig. 7 are obtained by setting $\lambda = m_{\tilde{\gamma}}/m_{\tilde{g}}$ to zero. It is interesting to note that the missing-p_T event rate increases with λ due to the boost effect: see Fig. 9 in Appendix D. Figure 8 shows the monojet cross section versus λ at $m_{\tilde{g}} = 5$ GeV. We find that even with the soft fragmentation of Eq. (11b) (dashed curves), the monojet cross section exceeds 0.1 nb for $\lambda > 0.75$ Hence we may conclude that $\lambda = m_{\tilde{\gamma}}/m_{\tilde{g}}$ should be either smaller than 0.75 or larger than 0.9 in the light-gluino scenario of Refs. 1 and 2.

The major conclusions of our analysis are that the light-gluino—heavy-scalar-quark scenario remains viable when fragmentation effects are taken into account and that Altarelli-Parisi evolution may well give a substantial

FIG. 5. Missing-p_T distribution from the subprocesses (1) and (2) in $p\bar{p}$ collisions at $\sqrt{s} = 540$ GeV for $m_{\tilde{g}} = 5$ GeV. Scalar-quark masses are infinite and $m_{\tilde{\gamma}} = 0$. The curves are obtained using the effective fragmentation function of Eq. (11a) (solid curves), Eq. (11b) (dashed curves), or neglecting fragmentation (dotted curves).
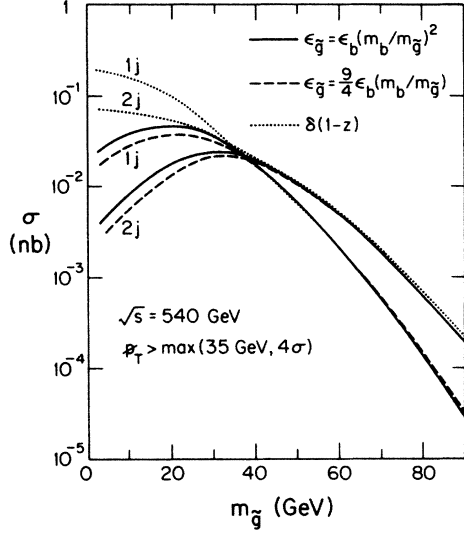
FIG. 7. Monojet and dijet cross section in $p\bar{p}$ collisions at $\sqrt{s} = 540$ GeV as functions of gluino mass. We set $m_{\tilde{\gamma}} = 0$ and $m_{\tilde{q}} = 100$ GeV; the contributions from $\tilde{q}\,\tilde{g}$ production, followed by $\tilde{q} \to q\tilde{g}$ or $\tilde{q} \to q\tilde{\gamma}$ decays, $\tilde{g}\,\tilde{g}$ production (1), and $g\tilde{g}$ production (2b) are summed. The curves are obtained by using the effective fragmentation function with Eq. (11a) (solid curves), with Eq. (11b) (dashed curves), and by neglecting fragmentation (dotted curves).
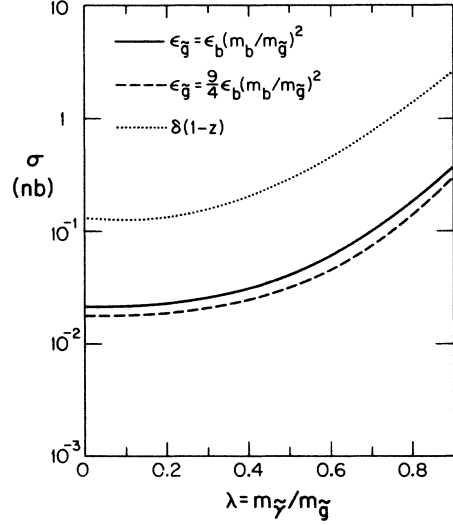

FIG. 8. Monojet cross section in $p\bar{p}$ collisions at $\sqrt{s} = 540$ GeV at $m_{\tilde{g}} = 5$ GeV, $m_{\tilde{q}} = 100$ GeV as a function of $\lambda = m_{\tilde{\gamma}}/m_{\tilde{g}}$. The curves are obtained by using the effective fragmentation function with Eq. (11a) (solid curves), with Eq. (11b) (dashed curve), and by neglecting fragmentation (dotted curve).

overestimate of the gluino distribution.

A potentially promising place to confirm the existence of light gluinos would be in the radiative decay of the Υ into a light-gluino ball.[21]

ACKNOWLEDGMENTS

APPENDIX A

In this appendix we review the method of successive approximations for solving the equations governing the Q^2 evolution of the singlet, gluon, and gluino distribution functions in a nucleon. The application of the method to the solution of the equations governing fragmentation functions follows straightforwardly.

To avoid singularities at the origin, we work with the distributions multiplied by a factor of x^2. Neglecting scalar-quark contributions, the equations for x^2 times the singlet, gluon, and gluino distributions become[8]

$$Q\frac{\partial}{\partial Q}q_s = \frac{\alpha_s(Q)}{\pi}(P_{qq}*q_s + 2fP_{qg}*g) ,\tag{A1a}$$

$$Q\frac{\partial}{\partial Q}g = \frac{\alpha_s(Q)}{\pi}(P_{gq}*q_s + P_{gg}*g + P_{g\tilde{g}}*\tilde{g}) ,\tag{A1b}$$

$$Q\frac{\partial}{\partial Q}\tilde{g} = \frac{\alpha_s(Q)}{\pi}(P_{\tilde{g}g}*g + P_{\tilde{g}\tilde{g}}*\tilde{g}) ,\tag{A1c}$$

where $q_s, g, \tilde{g}$ are the singlet, gluon, and gluino distributions multiplied by x^2, respectively, f is the number of quark flavors, and the star product is defined by

$$P_{ab}*f \equiv \int_x^1 \frac{dy}{y}\frac{x^2}{y^2}P_{ab}\left(\frac{x}{y}\right)f(y) .\tag{A2}$$

We choose[4]

$$\frac{\pi}{\alpha_s} = \tfrac{9}{2}\ln(Q/\Lambda) - \tfrac{1}{3}\sum_{q=c,b,t}\theta(Q - 2m_q)\ln(Q/2m_q)$$

$$- \theta(Q - 2m_{\tilde{g}})\ln(Q/2m_{\tilde{g}})\tag{A3}$$

with $\Lambda = 0.2444$ GeV. Note that between any two thresholds we can write

$$\frac{\pi}{\alpha_s} = b_f\ln(Q/\Lambda_f) ,\tag{A4}$$

where b_f and Λ_f are constants that can be determined from Eq. (A3). In the following we assume that Q lies in a region between thresholds so that Eq. (A4) is satisfied. Defining the variable

$$\bar{s} = \ln[\ln(Q/\Lambda_f)/\ln(Q_0/\Lambda_f)]$$

and using Eq. (A4) in Eqs. (A1) we obtain

$$\frac{dq_s}{d\bar{s}} = \frac{1}{b_f}(P_{qq}*q_s + 2fP_{qg}*g) ,\tag{A5a}$$

$$\frac{dg}{d\bar{s}} = \frac{1}{b_f}(P_{gq}*q_s + P_{gg}*g + P_{g\tilde{g}}*\tilde{g}) ,\tag{A5b}$$

$$\frac{d\tilde{g}}{d\bar{s}} = \frac{1}{b_f}(P_{\tilde{g}g}*g + P_{\tilde{g}\tilde{g}}*\tilde{g}) .\tag{A5c}$$

Integrating over $\bar{s}$ and imposing the boundary conditions

$$q_s(x,\bar{s}=0)=q_{s0}(x) ,\qquad\text{(A6a)}$$

$$g(x,\bar{s}=0)=g_0(x) ,\qquad\text{(A6b)}$$

$$\widetilde{g}(x,\bar{s}=0)=\widetilde{g}_0(x) ,\qquad\text{(A6c)}$$

we obtain

$$q_s(x,\bar{s})=\frac{1}{b_f}\int_0^{\bar{s}}d\bar{s}'(P_{qq}*q_s+2fP_{qg}*g)$$
$$+q_{s0}(x) ,\qquad\text{(A7a)}$$

$$g(x,\bar{s})=\frac{1}{b_f}\int_0^{\bar{s}}d\bar{s}'(P_{gq}*q_s+P_{gg}*g+P_{g\widetilde{g}}*\widetilde{g})$$
$$+g_0(x) ,\qquad\text{(A7b)}$$

$$\widetilde{g}(x,\bar{s})=\frac{1}{b_f}\int_0^{\bar{s}}d\bar{s}'(P_{\widetilde{g}g}*g+P_{\widetilde{g}\widetilde{g}}*\widetilde{g})+\widetilde{g}_0(x) .\qquad\text{(A7c)}$$

These equations are of the general form

$$\mathbf{V}=T\mathbf{V} ,\qquad\text{(A8)}$$

where $\mathbf{V}$ is a three-component vector function of x and $\bar{s}$ and T is a 3×3 linear matrix operator. Equation (A8) implies that $\mathbf{V}$ is a fixed point of the linear operator T. This suggests that we solve Eqs. (A7) using the method of successive approximations.[13] Starting from an initial guess, $\mathbf{V}^{(0)}$, we form the sequence of successive approximants $\mathbf{V}^{(1)}=T\mathbf{V}^{(0)}$, $\mathbf{V}^{(2)}=T\mathbf{V}^{(1)},\ldots,$ $\mathbf{V}^{(n)}=T\mathbf{V}^{(n-1)}$, etc. If the sequence $\mathbf{V}^{(1)},\mathbf{V}^{(2)},\ldots$ satisfies a convergence criterion, we take $\mathbf{V}^{(n)}$ to be our approximation to the true solution $\mathbf{V}$. In practice, we use the relative-error criterion

$$\max\left|\frac{\mathbf{V}^{(n)}-\mathbf{V}^{(n-1)}}{\mathbf{V}^{(n)}}\right|<0.01 ,\qquad\text{(A9)}$$

where the maximum is taken over the range of x and $\bar{s}$ of interest.

Comparing Eq. (A8) with Eqs. (A7), we see that the operator T is given by

$$T=\frac{1}{b_F}\int_0^{\bar{s}}d\bar{s}'P+\mathbf{V}_0(x)\qquad\text{(A10)}$$

where P is an x-dependent matrix integral operator. With the initial guess $\mathbf{V}^{(0)}=\mathbf{V}_0$ and (A10), it can be shown by induction that the nth approximant is given by

$$\mathbf{V}^{(n)}=\sum_{k=0}^{n}\left[\frac{\bar{s}}{b_f}\right]^k\frac{P^k\mathbf{V}_0}{k!} .\qquad\text{(A11)}$$

Thus, the approximate solution is obtained as a power series in $(\bar{s}/b_f)$. The solution of the evolution equations is reduced to the problem of evaluating the one-dimensional integrals $P^k\mathbf{V}_0$, $k=1,2,\ldots,n$. We use a cubic spline quadrature method[22] to accomplish this. Once the solutions are obtained they may be reparametrized in more convenient forms as we have done in Appendices B and C.

APPENDIX B

In this appendix we present our parametrizations for the gluino distributions discussed in Sec. II of the text. All the parametrizations have the form

$$\widetilde{g}(x,Q)=\bar{s}x^{a_1}(1-x)^{a_2}\exp(a_3+a_4x) .$$

Each a_i $(i=1,\ldots,4)$ is a polynomial in the variable $\bar{s}=\ln[\ln(Q/\widetilde{\Lambda})/\ln(Q_0/\widetilde{\Lambda})]$ where $Q_0=2m_{\widetilde{g}}$ and $\widetilde{\Lambda}=Q_0(0.2\text{ GeV}/Q_0)^{25/19}$.

(1) $m_{\widetilde{g}}=3$ GeV:

$$a_1=-1.24602-0.48549\bar{s} ,$$

$$a_2=6.37744-0.00246\bar{s} ,$$

$$a_3=-0.31532-1.81919\bar{s}-0.93868\bar{s}^2 ,$$

$$a_4=-1.70973-5.08218\bar{s}+2.33223\bar{s}^2 .$$

(2) $m_{\widetilde{g}}=5$ GeV:

$$a_1=-1.33139-0.4492\bar{s} ,$$

$$a_2=6.30712-0.045518\bar{s} ,$$

$$a_3=-0.55418-2.26574\bar{s} ,$$

$$a_4=-2.2188-3.89532\bar{s} .$$

These parametrizations are accurate to within 10% for the range $0.01\leq x\leq0.7$, $Q_0\leq Q\leq100$ GeV. For $x>0.7$, the distributions are negligibly small.

APPENDIX C

In this appendix we present our parametrizations for the gluino fragmentation functions discussed in Sec. III of the text. All the parametrizations have the form

$$D_{\widetilde{g}}(z,Q)=\left[\frac{a_0+a_1\hat{z}+a_2\hat{z}^2+a_3\hat{z}^3}{1+a_4\hat{z}+a_5\hat{z}^2}\right]^2 ,\qquad\text{(C1)}$$

where $\hat{z}=(20z-11)/9$. Each a_i $(i=0,1,\ldots,5)$ is a polynomial in the variable $\bar{s}=\ln[\ln(Q/\widetilde{\Lambda})/\ln(Q_0/\widetilde{\Lambda})]$ where $Q_0=2m_{\widetilde{g}}$, $\widetilde{\Lambda}=Q_0(0.2\text{ GeV}/Q_0)^{25/19}$.

(1) $\epsilon_{\widetilde{g}}=\epsilon_b(m_b/m_{\widetilde{g}})^2$, $m_{\widetilde{g}}=3$ GeV:

$$a_0=0.86464+2.17106\bar{s}-5.38154\bar{s}^2+3.91266\bar{s}^3 ,$$

$$a_1=-0.51753-7.6374\bar{s}+16.1124\bar{s}^2-14.309\bar{s}^3 ,$$

$$a_2=-0.470465+3.74446\bar{s}-3.58544\bar{s}^2+3.71445\bar{s}^3 ,$$

$$a_3=0.137742+0.99139\bar{s}-3.85026\bar{s}^2+2.89725\bar{s}^3 ,$$

$$a_4=-1.84552-0.956452\bar{s}+5.85575\bar{s}^2-7.67955\bar{s}^3 ,$$

$$a_5=0.955084+0.483771\bar{s}-2.72305\bar{s}^2+3.25267\bar{s}^3 .$$

(2) $\epsilon_{\widetilde{g}}=\frac{9}{4}\epsilon_b(m_b/m_{\widetilde{g}})^2$, $m_{\widetilde{g}}=3$ GeV:

$$a_0=1.07123+1.65569\bar{s}-7.43424\bar{s}^2$$
$$+13.9821\bar{s}^3-11.29951\bar{s}^4 ,$$

$$a_1=-0.742998-3.96398\bar{s}-13.80286\bar{s}^2$$
$$+75.4911\bar{s}^3-85.60941\bar{s}^4 ,$$

$$a_2 = -0.5885 + 3.921\,39\bar{s} + 0.692\,087\bar{s}^2$$
$$- 15.764\,94\bar{s}^3 + 22.281\bar{s}^4 ,$$

$$a_3 = 0.227\,831 - 0.471\,817\bar{s} + 10.2645\bar{s}^2$$
$$- 42.276\bar{s}^3 + 44.056\,35\bar{s}^4 ,$$

$$a_4 = -1.744\,45 + 1.766\,66\bar{s} - 19.6655\bar{s}^2$$
$$+ 71.2861\bar{s}^3 - 76.8651\bar{s}^4 ,$$

$$a_5 = 0.902\,701 + 0.301\,185\bar{s} - 1.187\,53\bar{s}^2$$
$$- 3.297\,43\bar{s}^3 + 8.472\,28\bar{s}^4 .$$

(3) $\epsilon_{\tilde{g}} = \epsilon_b (m_b/m_{\tilde{g}})^2$, $m_{\tilde{g}} = 5$ GeV:

$$a_0 = 0.655\,332 + 2.510\,67\bar{s} - 3.733\,99\bar{s}^2 ,$$

$$a_1 = -0.398\,226 - 6.556\,82\bar{s} + 7.372\,16\bar{s}^2 ,$$

$$a_2 = -0.342\,233 + 3.181\,51\bar{s} - 1.680\,71\bar{s}^2 ,$$

$$a_3 = 0.085\,393\,8 + 0.855\,102\bar{s} - 1.938\,49\bar{s}^2 ,$$

$$a_4 = -1.947\,83 - 0.058\,848\bar{s} + 0.406\,985\bar{s}^2 ,$$

$$a_5 = 0.985\,563 + 0.118\,398\bar{s} - 0.436\,595\bar{s}^2 .$$

(4) $\epsilon_{\tilde{g}} = \frac{9}{4}\epsilon_b (m_b/m_{\tilde{g}})^2$, $m_{\tilde{g}} = 5$ GeV:

$$a_0 = 0.824\,475 + 1.963\,84\bar{s} - 3.175\,08\bar{s}^2 ,$$

$$a_1 = -0.505\,765 - 6.396\,51\bar{s} + 7.361\,103\bar{s}^2 ,$$

$$a_2 = -0.443\,506 + 3.625\,45\bar{s} - 2.114\,69\bar{s}^2 ,$$

$$a_3 = 0.127\,724 + 0.706\,023\bar{s} - 1.781\,54\bar{s}^2 ,$$

$$a_4 = -1.886\,26 - 0.097\,914\,3\bar{s} + 0.597\,952\bar{s}^2 ,$$

$$a_5 = 0.966\,585 + 0.177\,333\bar{s} - 0.630\,935\bar{s}^2 .$$

These parametrizations reproduce the fragmentation functions to within 10% (except for regions where the fragmentation functions are quite small) for the range $0.1 \le z \le 1$, $Q_0 \le Q \le 100$ GeV.

APPENDIX D

In the calculation of various cross sections, it is necessary to evaluate many-dimensional integrals. These integrals can be considerably simplified by the introduction of a collinear approximation. This approximation is valid when $p_{\tilde{g}_h} \gg m_{\tilde{g}}$ where all the decay products of the gluino hadron $(\tilde{g}_h)$ have momenta collinear to the parent momentum in the laboratory frame. We can therefore integrate directly over transverse momenta and replace five-dimensional integrals over the three-body space for the decay $\tilde{g} \to q\bar{q}\tilde{\gamma}$ by an integral over a single collinear momentum variable. We will in the following derive the collinear decay function used in our calculations.

We define the scaling variables as

$$\lambda = \frac{m_{\tilde{\gamma}}}{m_{\tilde{g}}} , \tag{D1}$$

$$z \equiv \frac{2p_{\tilde{g}} \cdot p_{\tilde{\gamma}}}{m_{\tilde{g}}^2} . \tag{D2}$$

The photino energy distribution arising from the gluino decay $\tilde{g} \to q\bar{q}\tilde{\gamma}$ is then given in the massless-quark limit by[23]

$$\frac{dD}{dz} = F(z,\lambda) = 2f(\lambda)^{-1}(z^2 - 4\lambda^2)^{1/2}[z(3-2z) + 6(1-z)\lambda - (4-3z)\lambda^2 + 6\lambda^3] \tag{D3a}$$

with[2]

$$f(\lambda) = (1-\lambda^2)(1+2\lambda - 7\lambda^2 + 20\lambda^3 - 7\lambda^4 + 2\lambda^5 + \lambda^6) + 24\lambda^3(1-\lambda+\lambda^2)\ln(\lambda) . \tag{D3b}$$

The distribution (D3) is normalized such that

$$\int_{2\lambda}^{1+\lambda^2} dz\, F(z,\lambda) = 1 . \tag{D4}$$

Averaging over the polarization of the parent gluino, the invariant decay distribution can be expressed in terms of $F(z,\lambda)$ as

$$\frac{E\,dD}{d^3p} = \frac{1}{4\pi m_{\tilde{g}}^2} \frac{F(z,\lambda)}{(z^2 - 4\lambda^2)^{1/2}} . \tag{D5}$$

In the laboratory frame, we denote the $\tilde{g}_h$ momentum as P and the longitudinal and transverse components of the $\tilde{\gamma}$ momentum about the P direction as p_L and p_T, respectively. We define the longitudinal momentum fraction and the normalized transverse momentum of the photino as

$$\eta = p_L/P , \tag{D6a}$$

$$\xi_T = p_T/M , \tag{D6b}$$

with $M = m_{\tilde{g}_h} = m_{\tilde{g}}$. In the collinear limit $M^2/P^2 \to 0$, the $\tilde{\gamma}$ momentum becomes collinear to the $\tilde{g}_h$ momentum for finite η, since the $\tilde{\gamma}$ transverse momentum cannot be larger than $M/2$. In this limit, it is easy to obtain the relation between the laboratory-frame variables (D6) and the invariant variable z (D2),

$$z = \eta + \frac{\xi_T^2 + \lambda^2}{\eta} + O\left[\frac{M^2}{P^2}\right] . \tag{D7}$$

The kinematical region of the variables η and ξ_T in this limit reads

$$\lambda^2 < \eta < 1 , \tag{D8a}$$

$$0 < \xi_T^2 < (1-\eta)(\eta - \lambda^2) . \tag{D8b}$$

Now it is straightforward to obtain the collinear decay function by integrating over p_T:

LIGHT-GLUINO SCENARIO

$$\eta \frac{dD}{d\eta} = \int d^2p_T \frac{E\,dD}{d^3p} + O\left[\frac{M^2}{P^2}\right]$$

$$= \int_0^{(1-\eta)(\eta-\lambda^2)} d\xi_T^2 \frac{F(z,\lambda)}{(z^2-4\lambda^2)^{1/2}}$$

$$+ O\left[\frac{M^2}{P^2}\right] . \tag{D9}$$

The integral can be done analytically and gives

$$\frac{dD}{d\eta} = \frac{1}{3f(\lambda)}\left[G(1+\lambda^2) - G\left[\eta + \frac{\lambda^2}{\eta}\right]\right] \tag{D10a}$$

with

$$G(z) = z[12\lambda(3-2\lambda+3\lambda^2)+9(1-\lambda)^2 z - 4z^2] . \tag{D10b}$$

The normalization

$$\int_{\lambda^2}^1 d\eta \frac{dD}{d\eta} = 1 \tag{D11}$$

follows directly from Eqs. (D4) and (D9).

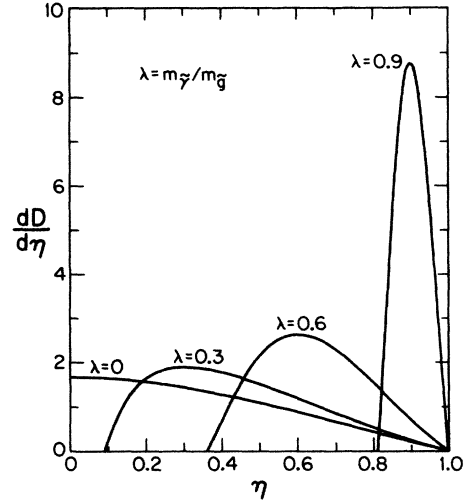We show in Fig. 9 the function $dD/d\eta$ for various values of λ. Note that $dD/d\eta$ vanishes at the boundaries

FIG. 9. Collinear decay function of Eq. (D10), with $\lambda = m_{\tilde\gamma}/m_{\tilde g} = 0$, 0.3, 0.6, and 0.9.

$\eta = \lambda^2$ and 1, and it approaches a δ function as $\lambda \to 1$. The rather important photino-mass effect under the boost is appropriately taken into account in the collinear approximation.

[1]M. J. Herrero, L. E. Ibáñez, C. López, and F. J. Yndurain, Phys. Lett. 132B, 199 (1983); 145B, 430 (1984).

[2]V. Barger, K. Hagiwara, W.-Y. Keung, and J. Woodside, Phys. Rev. Lett. 53, 641 (1984).

[3]G. Arnison et al. (UA1 Collaboration), Phys. Lett. 139B, 115 (1984).

[4]V. Barger, K. Hagiwara, W.-Y. Keung, and J. Woodside, Phys. Rev. D 31, 528 (1985).

[5]E. Reya and D. P. Roy, Phys. Lett. 141B, 442 (1984); Phys. Rev. Lett. 52, 881 (1984); J. Ellis and H. Kowalski, Phys. Lett. 142B, 441 (1984).

[6]V. Barger, K. Hagiwara, and W.-Y. Keung, Phys. Lett. 145B, 147 (1984); J. Ellis and H. Kowalski, Nucl. Phys. B246, 189 (1984); A. R. Allan, E. W. N. Glover, and A. D. Martin, Phys. Lett. 146B, 247 (1984); see also H. E. Haber and G. L. Kane, ibid. 142B, 212 (1984).

[7]See, e.g., K. Inoue, A. Kakuto, H. Komatsu, and S. Takeshita, Prog. Theor. Phys. 67, 1889 (1982); C. Kounnas, A. B. Lahanas, D. V. Nanopoulos, and M. Quiros, Nucl. Phys. B236, 438 (1984).

[8]B. A. Campbell, J. Ellis, and S. Rudaz, Nucl. Phys. B198, 1 (1982); I. Antoniadis, C. Kounnas, and R. Lacaze, ibid. B211, 216 (1983); C. Kounnas and D. A. Ross, ibid. B214, 317 (1983); S. K. Jones and C. H. Llewellyn Smith, ibid. B217, 145 (1983).

[9]M. Barnett, H. Haber, and G. Kane, Phys. Rev. Lett. 54, 1983 (1985).

[10]A. De Rújula and R. Petronzio, CERN Report No. TH-4070, 1984 (unpublished).

[11]E. Witten, Nucl. Phys. B104, 445 (1976); L. F. Abbott and M. B. Wise, ibid. B176, 373 (1980).

[12]G. Altarelli and G. Parisi, Nucl. Phys. B126, 298 (1977).

[13]I. Stakgold, Green's Functions and Boundary Value Problems (Wiley, New York, 1979).

[14]E. Eichten, I. Hinchliffe, K. Lane, and C. Quigg, Rev. Mod. Phys. 56, 579 (1984); K. Hagiwara and S. Jacobs (in preparation).

[15]J. F. Owens, Phys. Lett. 76B, 85 (1978); T. Uematsu, ibid. 79B, 97 (1978).

[16]C. Peterson, D. Schlatter, I. Schmitt, and P. M. Zerwas, Phys. Rev. D 27, 105 (1983).

[17]J. M. Izen, DESY Report No. 84-104 (unpublished).

[18]C. Weizsäcker and E. J. Williams, Z. Phys. 88, 612 (1934).

[19]M. Glück, E. Hoffman, and E. Reya, Z. Phys. C 13, 119 (1982).

[20]S. Dawson, Nucl. Phys. B249, 42 (1985); G. Kane, W. Repko, and W. Robnick, Phys. Lett. 148B, 367 (1984).

[21]W. Y. Keung and A. Khare, Phys. Rev. D 29, 265 (1984); J. H. Kühn and S. Ono, Phys. Lett. 142B, 436 (1984); T. Goldman and H. Haber, Physica 15D, 181 (1985); S. Ono, T. Yanagida, and S. Yazaki, University of Tokyo Report No. UT-443, 1984 (unpublished); J. H. Kühn, Phys. Lett. 151B, 174 (1985).

[22]G. Forsythe, M. Malcolm, and C. Moler, Computer Methods for Mathematical Computations (Prentice-Hall, Englewood Cliffs, N.J., 1977).

[23]H. Haber and G. L. Kane, Nucl. Phys. B232, 333 (1984).